

PACS numbers: 42.55.Rz; 42.60.Lh
DOI: 10.1070/QE2009v039n09ABEH014036

Amplification of laser radiation in disk Yb : YAG crystals cooled down to the liquid nitrogen temperature

E.A. Perevezentsev, I.B. Mukhin, O.V. Palashov, E.A. Khazanov

Abstract. **The parameters of a diode-pumped Yb : YAG amplifier are calculated. The derived expressions allow one to determine the optimal doping of the YAG crystal with Yb ions, which is $\sim 10\,\%$ for a 600-μm-thick crystal. The calculations take into account the absorption line profile and the characteristics of the pump spectrum (the shape, width, central wavelength). When the 10 % Yb-doped YAG crystal is cooled down from 296 K to 80 K, the shift of the gain profile centre (~ 0.3 nm) and the increase in the stimulated emission cross section (by four times) as well as the depletion of the lower working level are observed. The small-signal gain (the maximum value is 1.7, which corresponds to the gain 4.4 cm^{-1}) is measured as a function of the absorbed pump power and well agrees with the results of theoretical calculations.**

Keywords: *disk laser, gain, cryogenic temperatures.*

1. Introduction

One of the most important directions in quantum electronics is the development of lasers with a high average and peak output power. The example of applications of these lasers is pumping of a wideband parametric amplifier [1] and controlled thermonuclear fusion [2 – 4].

One of the main factors restricting the average power is the heat release in active elements (AEs) leading to the following negative thermal effects: appearance of a thermal lens and thermal depolarisation of radiation [5, 6], and the increase in the temperature average in the volume, which lead to broadening and shift of emission lines, the decrease in the stimulated emission cross section at the active transition [7 – 9]. The strongest heat source in AEs of solid-state lasers is pump radiation. The heat-release power in neodymium lasers achieves tens of percent [10, 11] due to a large quantum defect of the pump, parasitic absorption processes in the excited state, cross relaxation, etc. [12]. In this connection, the ytterbium ion, which is characterised by a small quantum defect (10 %) [11, 13], the large inversion lifetime and the absence of absorption from the excited state [7 – 9], is widely used as an active ion. The use of AEs in the form of a thin disk is also promising [14, 15]. This geometry substantially decreases thermal distortions of radiation due to the end heat release at which the temperature gradient is directed along and not across the radiation propagation direction. In addition, the small length of the AE makes it possible to amplify short high-power pulses in the absence of self-focusing. Another method for suppressing thermal effects is the cooling of AEs down to the liquid nitrogen temperature [16 – 20]. In this case, the thermal and laser constants of the substance improve and the medium becomes a four-level one [7 – 9].

At present, in the world there exist several projects on designing high-power pulse periodic lasers based on Yb-doped crystals [21 – 24]. In this case, the pulse repetition rate is either small (10 Hz) or high (80 kHz). In this paper, we calculated the main parameters of a cryogenic disk Yb : YAG amplifier with the pulse repetition rate inverse to the inversion lifetime (1 kHz). We derived a set of approximate analytic solutions for the inverse populations and found the domains of their applicability. We determined the optimal concentration of Yb ions and took into account the linewidths of the pump radiation and absorption in AEs. We experimentally measured the dependences of the spectrum of the stimulated emission cross section and the small-signal gain on the pump power, which demonstrate an improvement of laser properties of the crystal upon its cooling. The experimental data and the results of theoretical calculations were compared.

2. Calculation of the population difference for working levels in AEs

Consider the following model. Pump radiation in the form of rectangular pulses of intensity I_0, duration t_0, and repetition rate T (the particular case $T = t_0$ corresponds to the cw regime) is incident (along the z axis) on the AE end face of thickness L and diameter d ($L \ll d$) (Fig. 1). We will consider the single-pass and double-pass geometries: pump radiation either passes through the AE or is reflected from its rear end without losses. Consider a short amplified laser pulse passing through the crystal at the moment of the pump pulse termination ($t = t_0$). The change in the difference in the populations of working levels $\Delta N(z, t)$ can be divided into three stages: accumulation within the pump pulse ($0 < t < t_0$), jump-wise decrease during the laser pulse amplification ($t = t_0$) and decrease due to spontaneous radiation ($t_0 < t < T$).

Let us make an assumption, standard for a four-level

E.A. Perevezentsev, I.B. Mukhin, O.V. Palashov, E.A. Khazanov Institute of Applied Physics, Russian Academy of Sciences, ul. Ul'yanova 46, 603950 Nizhnii Novgorod, Russia; e-mail: eperevezentsev@gmail.com

Received 26 December 2008; revision received 12 May 2009
Kvantovaya Elektronika **39** (9) 807 – 813 (2009)
Translated by I.A. Ulitkin

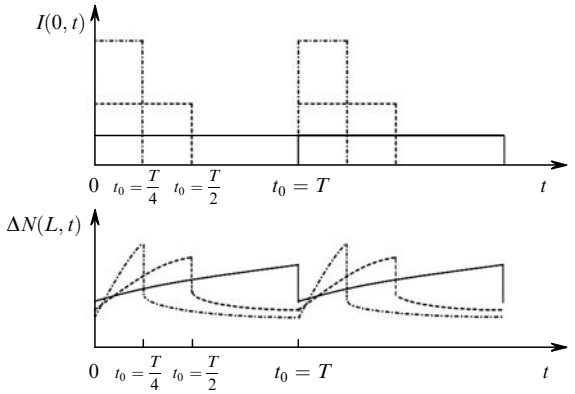

Figure 1. Time dependences of the pump radiation intensities $I(0,t)$ and difference in the populations of the working transition levels $\Delta N(L,t)$ at $t_0 = T$ (solid curves), $t_0 = T/2$ (dashed curves) and $t_0 = T/4$ (dash-and-dot curves).

scheme, about the lifetime of ions at different levels: $\tau_1, \tau_3 \ll \tau_2 = \tau$, where τ_k is the lifetime at the kth level (Fig. 2). First, we will solve the problem for the case of monochromatic pumping and then will take into account the linewidths of pump radiation and absorption.

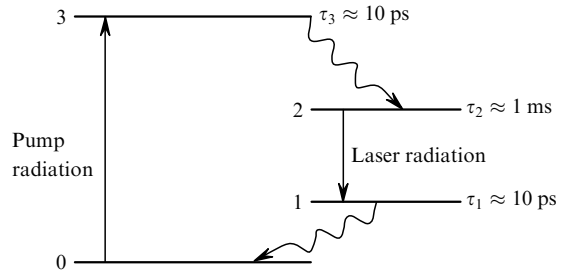

Figure 2. System of AE levels.

2.1 Case of a single-pass geometry

In this case, the system of balance equations during $t = [0, t_0]$ for the difference in populations ΔN_1 and intensity I_1 of the monochromatic pump has the form

$$\frac{\partial I_1(z,t)}{\partial z} = \sigma[\Delta N_1(z,t) - N_0] I_1(z,t),$$
$$\frac{\partial \Delta N_1(z,t)}{\partial t} = -\frac{I_1(z,t)}{I_s \tau}[\Delta N_1(z,t) - N_0]\frac{\Delta N_1(z,t)}{\tau}, \quad (1)$$

where I_s and σ are the saturation intensity and stimulated emission cross section at the pump transition; N_0 is the concentration of activator ions in the crystal. We will integrate the first equation of system (1) in z from 0 to z, will substitute I_1 into the second equation of this system and will integrate it again in z from 0 to z. As a result, we obtain

$$\frac{\partial \sigma N_1(z,t) z}{\partial t}\tau = \rho\{1 - \exp[\sigma N_1(z,t) z - \sigma N_0 z]\} - \sigma N_1(z,t) z, \quad (2)$$

where $\rho = I_0/I_s = \text{const}$;

$$N_1(z,t) = \frac{1}{z}\int_0^z \Delta N_1(\xi,t)\mathrm{d}\xi. \quad (3)$$

Laser pulse amplification is determined by the small-signal gain

$$\exp\left(\sigma_{las}\int_0^L \Delta N_1(\xi,t)\mathrm{d}\xi\right) = \exp[\sigma_{las} N_1(L,t_0) L],$$

where σ_{las} is the stimulated emission cross section at the working laser transition.

Equation (2) is solved only in quadratures but in a number of cases it can turn out that $\sigma N_1(z,t) z \ll 1$ is a small parameter. Then, we obtain from (2)

$$\frac{\partial \sigma N_{11}(z,t) z}{\partial t}\tau = \rho[1 - \exp(-\sigma N_0 z)] - \sigma N_{11}(z,t) z \rho \times \exp(-\sigma N_0 z) - \sigma N_{11}(z,t) z, \quad (4)$$

where $N_{11}(z,t)$ is the solution of Eqn (2) with a partial allowance for the saturation effect. The three terms in the right-hand side of Eqn (4) are responsible for pumping, saturation, and spontaneous emission, respectively. In particular, equation (4) without the second term in the right-hand side is derived from (1), if saturation is absent, i.e. when $I_1(z,t) = I_1(0,t)\exp(-\sigma N_0 z)$.

The change in the difference of the populations ΔN_1 is periodic in time with the period T, and hence, it is necessary to specify the conditions coupling its values at the period bountdaries, i.e. at $t = 0$ and $t = T$. Strictly speaking, in this case it is necessary to use the Frantz–Nodvik formula [25] for the specific laser pulse energy. We will restrict our consideration to simplified boundary conditions: when the amplified pulse propagates, the quantity N_1 decreases by $1/h$ times at each point of the crystal, i.e.

$$N_1(z,0) = h(z) N_1(z,t_0)\exp\left(\frac{t_0 - T}{\tau}\right). \quad (5)$$

Expression (4), taking into account boundary condition (5), has the exact solution

$$N_{11}(z,t) = \frac{a_1(z)}{a_0(z)+1}\left\{\left[h(z)\exp\left(-\frac{T-t_0}{\tau}\right) - 1\right] \times \exp\left\{-\frac{t}{\tau}[a_0(z)+1]\right\} \times \left\{1 - h(z)\exp\left[-\frac{t_0 a_0(z) + T}{\tau}\right]\right\}^{-1} + 1\right\}, \quad (6)$$

where

$$a_0(z) = \rho\exp(-\sigma N_0 z);\ a_1(z) = \frac{\rho[1 - \exp(-\sigma N_0 z)]}{\sigma z}. \quad (7)$$

In addition, it is easy to obtain the solution of Eqn (4) by neglecting the spontaneous emission (N_{11i}), saturation (N_{11t}) and both effects (N_{110}):

$$N_{11i}(z,t) = \frac{a_1(z)}{a_0(z)}\left\{\left[h(z)\exp\left(-\frac{T-t_0}{\tau}\right) - 1\right] \times \exp\left[-\frac{t}{\tau}a_0(z)\right] \times$$

$$\times\left\{1-h(z)\exp\left[-\frac{t_0}{\tau}\,a_0(z)-\frac{T-t_0}{\tau}\right]\right\}^{-1}+1\Bigg\}, \quad (8)$$

$$N_{11t}(z,t)=a_1(z)\left\{\left[h(z)\exp\left(-\frac{T-t_0}{\tau}\right)-1\right]\exp\left(-\frac{t}{\tau}\right)\right.$$

$$\left.\times\left[1-h(z)\exp\left(-\frac{T}{\tau}\right)\right]^{-1}+1\right\}, \quad (9)$$

$$N_{110}(z,t)=a_1(z)\left\{\frac{t}{\tau}+\frac{t_0}{\tau}\,h(z)\exp\left(-\frac{T-t_0}{\tau}\right)\right.$$

$$\left.\times\left[1-h(z)\exp\left(-\frac{T}{\tau}\right)\right]^{-1}\right\}. \quad (10)$$

Here, we do not define under what conditions we can use either this or that approximation; this problem will be discussed below.

The term responsible for the spontaneous emission can be also selected in exact equation (2). The general solution of (2) by neglecting the spontaneous emission has the form

$$N_{1i}(z,t)=N_0-\frac{1}{\sigma z}\ln\left[c_1(z)\exp\left(-\frac{t}{\tau}\,\rho\right)+1\right], \quad (11)$$

where the integration constant $c_1(z)$ under boundary conditions (5) is the solution of the transcendental equation

$$\sigma N_0 z-\ln[c_1(z)+1]=\left\{\sigma N_0 z\right.$$

$$\left.-\ln\left[c_1(z)\exp\left(-\frac{t_0}{\tau}\,\rho\right)+1\right]\right\}h(z)\exp\left(-\frac{T-t_0}{\tau}\right). \quad (12)$$

We will assume below that $h=1/2=\text{const}$. Then, in the case of cw pumping ($t_0=T$), we have

$$c_1(z)=\frac{1}{2}\left\{\exp\left(-\frac{t_0}{\tau}\,\rho+\sigma N_0 z\right)-2\right.$$

$$\left.+\left\{\left[2-\exp\left(-\frac{t_0}{\tau}\,\rho+\sigma N_0 z\right)\right]^2-4[1-\exp(\sigma N_0 z)]\right\}^{1/2}\right\}. \quad (13)$$

For clearness, the set of solutions of system (1) is presented in Table 1.

Table 1. A set of solutions of systems of equations (1) and (14).

Saturation	Spontaneous emission	
	Taken into account	Neglected
Taken into account	N_1, N_2 (exact numerical solution)	N_{1i} (11)–(13), N_{2i}
Taken into account approximately [expansion in $\sigma\Delta N_1(z,t)z\ll 1$]	N_{11} (6), (7), N_{21}	N_{11i} (8), N_{21i}
Neglected	N_{11t} (9), N_{21t}	N_{110} (10), N_{210}

2.2 Case of a double-pass geometry

In this case, the system of balance equations during $t=[0,t_0]$ for the difference in the populations ΔN_2 has the form

$$\frac{\partial I_1(z,t)}{\partial z}=\sigma[\Delta N_2(z,t)-N_0]I_1(z,t),$$

$$\frac{\partial I_2(z,t)}{\partial z}=-\sigma[\Delta N_2(z,t)-N_0]I_2(z,t), \quad (14)$$

$$\frac{\partial\Delta N_2(z,t)}{\partial t}=-\frac{I_1(z,t)+I_2(z,t)}{I_s\tau}[\Delta N_2(z,t)-N_0]-\frac{\Delta N_2(z,t)}{\tau},$$

where $I_1(z,t)$ and $I_2(z,t)$ are the intensities of monochromatic pump radiation incident on the crystal and reflected from the mirror, respectively. Reflection from the mirror will be assumed ideal, i.e. $I_1(L,t)=I_2(L,t)$.

Similarly to the case of the single-pass geometry, we obtain from (14) the equation for $N_2(z,t)$:

$$\frac{\partial\sigma N_2(z,t)z}{\partial t}\,\tau=\rho\{1-\exp[\sigma N_2(z,t)z-\sigma N_0 z]\}$$

$$+\rho\{\exp[2\sigma N_2(L,t)L-2\sigma N_0 L]$$

$$\times\{\exp[-\sigma N_2(z,t)z+\sigma N_0 z]-1\}\}-\sigma N_2(z,t)z. \quad (15)$$

Equation (15) at $z=L$ coincides with equation (2) with the accuracy to substitution $\sigma\to 2\sigma$, $I_s\to I_s/2$, and, hence, the function $N_2(L,t)$ entering (15) can be found from section 2.1 with the help of the mentioned substitution and by setting boundary conditions (5) with the replacement of subscript 1 by subscript 2. By expanding the right-hand side of (15) in the small parameter $2\sigma N_2(z,t)z\ll 1$, we obtain a set of solutions similar to (6)–(13): the exact solution N_{21}, the solutions obtained by neglecting the spontaneous emission N_{21i}, by neglecting saturation N_{21t}, and by neglecting both these effects N_{210}. Similarly, the spontaneous emission in (15) being neglected, we obtain $N_{2i}(L,t)$.

3. Analysis of the obtained solutions

We will analyse the results of calculations by specifying the given parameters of the YAG:Yb active medium at 80 K: $\tau=1$ ms, $\sigma=1.7\times10^{-20}$ cm^2, $I_s=14$ kW cm^{-2}, $\sigma_{las}=7.56\times10^{-20}$ cm^2, $L=600$ μm and the pump parameters: $d=6$ mm, $T=1$ ms, $h=1/2$. The average pump power $P_0=t_0I_0\pi d^2/(4T)=1$ kW is assumed the same independently of the off-duty ratio t_0/T.

First of all, we will find the domains of applicability of the solutions obtained and then will determine the optimal atomic concentration of Yb (1 % doping by Yb ions corresponds to their concentration $N_0=1.38\times10^{20}$ cm^{-3}) and take into account the finite width of the Yb absorption line.

3.1 Domain of applicability of approximate solutions

The pump pulse duration t_0 is comparable with the lifetime τ at the upper working level, and hence, saturation cannot be neglected. Analysis of the time dependences of the logarithmic gain $\sigma_{las}N_2(L,t)L$ for the solutions taking into account the spontaneous emission (N_2, N_{21} and N_{21t}) at $t_0=T$, $T/2$, $T/4$ shows that at the 10 % doping (see section 3.2 below), $N_2\approx N_{21}$ (the difference is less than 0.1 %), and N_{21t} slightly differs from N_2 (less than by 2 %). Thus, below the solution with the approximate allowance for the saturation is assumed exact to some degree and we will compare only N_{21} with N_{21t}.

Note that the inequality $N_2<N_{21}<N_{21t}$ is always fulfilled: more exact we take saturation into account, the

less the difference in the populations of working levels. Below we will consider all the dependences at the moment of arrival of the amplifying pulse ($t = t_0$).

Compare the values of $N(L, t_0)$ obtained in different approximations. This quantity was selected because it determines the small-signal gain $\exp[\sigma_{las} N(L, t_0)L]$ at the moment of arrival of the amplifying pulse. As was noted above, the values of $N(L, T)$ for the cases of single-pass and double-pass geometries coincide with the accuracy to substitution $\sigma \to 2\sigma$, $I_s \to I_s/2$ and, hence it is sufficient to consider only a more interesting case of the double-pass geometry. We will compare $N_{21}(L, T)$ with $N_2(L, T)$ to find the regions in which we can perform expansion in the small parameter ($2\sigma N_2(z, t)z \ll 1$). We will find the domains of applicability of solutions $N_{21i}(L, T)$, $N_{21t}(L, T)$, $N_{210}(L, T)$, and $N_{2i}(L, T)$ by comparing $N_{21i}(L, T)$, $N_{21t}(L, T)$, and $N_{210}(L, T)$ with $N_{21}(L, T)$, and $N_{2i}(L, T)$ with $N_2(L, T)$. The difference less than 5 % between the quantities being compared will be assumed to be the criterion for the approximation operability. We will restrict our consideration to cw pumping ($t_0 = T$) and set $2\sigma N_0 L = 2.82$, which corresponds to 10 % doping by Yb. This problem contains only two parameters: ρ and T/τ. Figre 3 shows the domains of applicability of solutions in the plane ρ, T/τ.

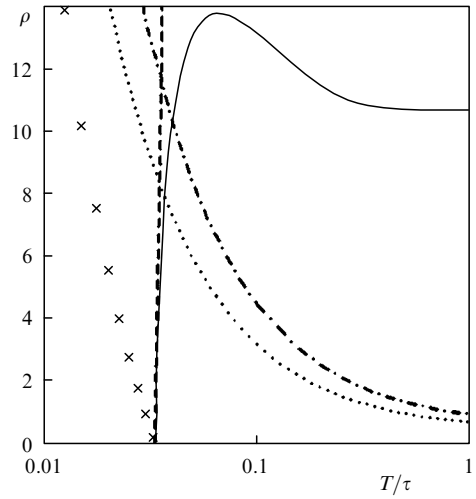

Figure 3. Domains of applicability of obtained approximate solutions of equation (15) in the plane $\rho, T/\tau$ at $2\sigma N_0 L = 2.82$. In the domain on the left from the dash-and-dot curve, we can use the solution $N_{21}(z, t)$, on the left from the dashed and dash-and-dot curves simultaneously – the solution $N_{21i}(z, t)$, on the left from the dotted curve – the solution $N_{21t}(z, t)$, on the left from the cross curve – the solution $N_{210}(z, t)$. Below the solid curve and above the dash-and-dot curve, it is necessary to use the numerical solution of equation (15) to obtain the accuracy above 5 %.

Let us explain the shapes of the curves restricting these domains from the physical point of view. In the domain on the left of the dashed and dash-and-dot curves, the saturation effect can be partially or completely neglected. At $T \sim \tau$, the saturation can be neglected if the pump intensity does not exceed greatly the saturation intensity. At $T \ll \tau$, it is necessary to compare the energy density of the pump pulse $I_0 t_0$ with the energy density of saturation $E_s = I_s \tau$. Below we will explain the shape of the solid curve. Spontaneous emission can be neglected if $T \ll \tau$ or if the pump intensity is so large that the losses in inversion due to spontaneous emission are made up for.

Analysing the obtained domains, we can single out one more interesting fact: along the dash-and-dot curve, the parameter $2\sigma N_2(L, T)L = 1.24 - 1.37$. Thus, the solution formally obtained when this parameter is much smaller than unity, is valid in a much greater domain. This fact is explained as follows. Equation (15) at $z = L$ takes the form

$$\frac{\partial 2\sigma N_2(L, t)L}{\partial t}\tau = 2\rho - 2\rho \exp[2\sigma N_2(L, t)L - 2\sigma N_0 L] - 2\sigma N_2(L, t)L. \quad (16)$$

At $2\sigma N_0 L = 2.82$ and $2\sigma N_2(L, t)L = 1.24 - 1.37$, the contribution of the second term is much smaller than that of the first one, and the error, appearing due to incorrect expansion of the exponential, is small.

3.2 Selection of crystal parameters

The pump efficiency with respect to the stored energy η_s is determined as the ratio of the energy stored in the AE to the pump energy at the AE input

$$\eta_s = \frac{E_s \sigma_{las} N_2(L, t)L}{I_0 t_0}, \quad (17)$$

where $E_s = 2.5$ J cm^{-2}.

Figure 4 shows the dependences of η_s on Yb doping. One can see that the effect of saturation at $d = 6$ mm is small. When the average pump power is retained, the decrease in t_0 leads to an increase in the stored energy because losses on spontaneous emission decrease but this increase is not proportional to the peak pump power. From the point of view of material expenditures, it is more profitable to use the cw regime.

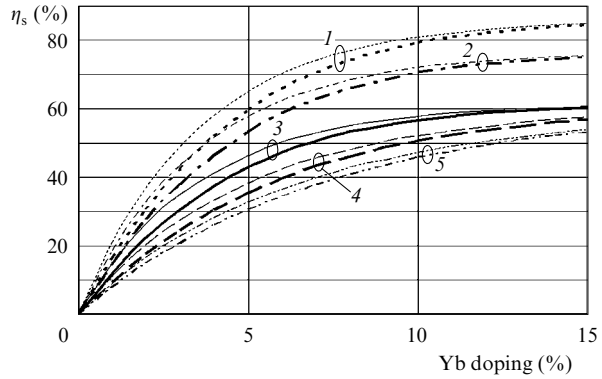

Figure 4. Dependences of the pump efficiency with respect to the stored energy η_s on Yb doping for different pulse duration t_0 and widths of the pump spectrum $\Delta\lambda$ on optimal wavelengths $\lambda_{0\,opt}$ by neglecting saturation (thin curves) and taking saturation into account at $d = 6$ mm (heavy curves): $t_0 = T/4$, $\Delta\lambda = 0$ (*1*), $t_0 = T/2$, $\Delta\lambda = 0$ (*2*), $t_0 = T$, $\Delta\lambda = 0$ (*3*), $t_0 = T$, $\Delta\lambda = 2.5$ nm (*4*), and $t_0 = T$, $\Delta\lambda = 5$ nm (*5*).

When Yb doping exceeds 10 %, the increase in the stored energy virtually stops (Fig. 4). However, the increase in the concentration deteriorates the optical properties and decreases the thermal conductivity of the crystal. In addition, the gain distribution, and thus the power density of the heat release become strongly inhomogeneous with respect to z. This can result in amplified spontaneous emission in the transverse direction and in an increase in negative thermal effects.

Thus, taking into account the results obtained above, it is reasonable to select Yb doping into the AE equal to $\sim 10\,\%$ and the pump regime – continuous. In this case, $\eta_s \sim 50\,\%$ (Fig. 4), i.e. at the average pump power of 1 kW, the pulse repetition rate of 1 kHz, and $h = 1/2$, the energy of one laser pulse is 250 mJ.

3.3 Account for the widths of the absorption line and the pump spectrum

Let the pump spectrum be Gaussian, i.e. $I = I_0 g(\lambda, \lambda_0, \Delta\lambda)$, where

$$g(\lambda, \lambda_0, \Delta\lambda) = \frac{2}{\Delta\lambda}\left(\frac{\ln 2}{\pi}\right)^{1/2} \times \exp\left[-4(\ln 2)\left(\frac{\lambda}{\lambda_0}\right)^2\left(\frac{\lambda-\lambda_0}{\Delta\lambda}\right)^2\right]; \quad (18)$$

λ_0 is the central wavelength of pump radiation; $\Delta\lambda$ is its spectrum width. Consider first the single-pass pump geometry. In this case, we assume that pump radiation consists of several monochromatic waves $(\lambda_1, \lambda_2, \ldots, \lambda_N)$ with the intensities $I_1', I_2', \ldots, I_N'$. Then, the system of balance equation during $t = [0, t_0]$ will have the form

$$I_1'(z,t) = I_1'(0,t)\exp\left\{\int_0^z \sigma(\lambda_1)[\Delta N_1(\xi,t) - N_0]\mathrm{d}\xi\right\},$$
$$\ldots\ldots\ldots\ldots\ldots\ldots\ldots\ldots\ldots\ldots\ldots\ldots$$
$$I_N'(z,t) = I_N'(0,t)\exp\left\{\int_0^z \sigma(\lambda_N)[\Delta N_1(\xi,t) - N_0]\mathrm{d}\xi\right\}, \quad (19)$$
$$\frac{\partial \Delta N_1(z,t)}{\partial t} = -\sum_{k=1}^{N}\frac{I_k'(z,t)}{I_{sk}\tau}[\Delta N_1(z,t) - N_0] - \frac{\Delta N_1(z,t)}{\tau},$$

where $I_{sk} = I_s(\lambda_{max})\,\sigma(\lambda_{max})/\sigma(\lambda_k)$; λ_{max} is the wavelength corresponding to the maximum of the function $\sigma(\lambda)$.

Passing to the continuous spectrum and replacing in equation (19) the sum by the integral, we obtain the solutions of this equation in the form of expression (6)–(10) but with the substitution of $a_{0,1}(z)$ by $\int_0^\infty a_{0,1}(z)\,\mathrm{d}\lambda$ in them. The solutions for the double-pass pump geometry are found similarly. However, in this case we failed to find the analytic solution, when the spontaneous emission is neglected.

Let us calculate η_s taking into account the shapes of the pump and absorption bands. For the absorption spectrum $\sigma(\lambda)$, we used data borrowed from paper [26]. We will find the optimal central pump wavelength $\lambda_0 = \lambda_{0opt}$ at which the maximum energy is stored in the AE. By plotting the level lines η_s as functions of Yb doping and the central wavelength λ_0, we found λ_{0opt} at the fixed 10 % Yb doping. As an example, Fig. 5 demonstrates the level lines η_s for the pump spectrum width $\Delta\lambda = 2.5$ nm, which corresponds to the experiment (see below). One can see from Fig. 5 that $\lambda_{0opt} = 940.5$ nm. It follows from a similar plot constructed at $\Delta\lambda = 5$ nm that $\lambda_{0opt} = 939$ nm. For these two values of λ_{0opt}, Fig. 4 shows the dependences of η_s on the Yb doping taking into account the shapes of the pump and absorption bands. One can see that the line profiles affect the quantity η_s much stronger than saturation and the effect of saturation is almost the same for different linewidths of pump radiation.

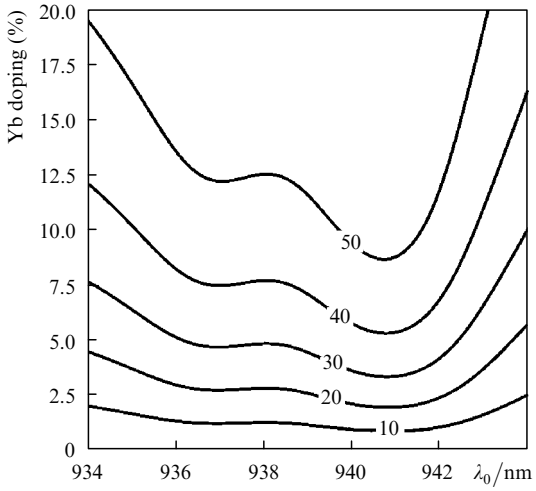

Figure 5. Level lines η_s (in percent) as functions of Yb doping and the central pump wavelength λ_0 with its spectrum width $\Delta\lambda = 2.5$ nm at $t_0 = T$.

4. Experimental investigation of the properties of the Yb:YAG crystal upon its cooling down to 78 K

4.1 Scheme of the experiment

Figure 6 shows the scheme of the experiment. The Yb:YAG crystals (10 % doping) represented thin disks of diameter 10 mm and thickness 400–900 μm. One of the faces had a dielectric AR coating and a mirror reflecting radiation at two wavelengths – 940 nm (pump radiation) and 1030 nm (laser radiation) – was deposited on the other face. Thus, radiation in all the experiments propagated twice though the crystal. In the master oscillator, the pump source was a 210-W JOLD-210-CAXF-6A cw diode laser (Germany) emitting the line of width ~ 3 nm at 935–940 nm. In the amplifier, the pump source was a 600-W LDM 100–600 diode laser (Germany) emitting the line of width ~ 2.5 nm at 935–940 nm. The power was measured with Gentec UP55N-400W-H9-D0 (30–400 W) and Gentec

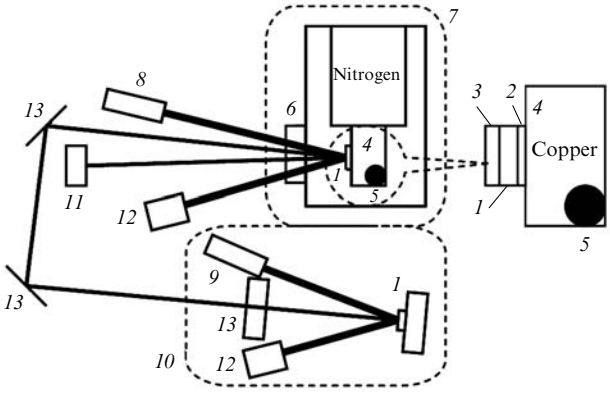

Figure 6. Scheme of the experimental setup: (*1*) Yb:YAG crystals; (*2*) indium layer; (*3*) sapphire disk; (*4*) copper heatsink; (*5*) thermocouple; (*6*) output window; (*7*) vaccum cryogenic chamber; (*8*, *9*) diode pump lasers; (*10*) master oscillator; (*11*) power meter; (*12*) screen; (*13*) mirror; thin line is the beam emitted by the oscillator ($\lambda \sim 1030$ nm); heavy lines are the beams emitted by diode lasers ($\lambda \sim 940$ nm).

UP19K-50L-H5-BT (0 – 50 W) power meters. The crystals were placed in optical cryostat (*7*) representing a vacuum chamber in a two-wall cooling vessel, which consisted of an internal vessel having a direct thermal contact with the sample under study and cooled by liquid nitrogen, and an external vessel used for producing vacuum. Pump radiation and radiation from the master oscillator were incident on the crystal through input window (*6*). The temperature of the copper heatsink was measured with thermal sensor (*5*). In experiments at room temperature, water was used for cooling. All the optical elements through which pump radiation propagated were made of fused quartz with a low absorption coefficient ($\sim 10^{-5}$ cm^{-1}) and the optical surfaces had AR coatings with the reflection coefficient less than 0.5 %. By using a set of lenses the pump beam diameter could be varied within 1.2 – 6 mm.

4.2 Change in the laser properties of the crystal during cooling

In the first experiment we measured the fraction of absorbed pump power η_p as a function of the temperature of a 600-μm-thick crystal placed in a cryogenic chamber. By cooling the crystal down from 296 K to 80 K, η_p increased from 75 % to 84 % at 939.5 nm, which indicates the increase in the absorption cross section of Yb ions at this wavelength.

To perform next experiments, on the basis on the linear resonator we fabricated an oscillator with the output power up to 1 W, the emission bandwidth of 0.5 nm and the wavelength tunable with the help of Wood's filter [27] in the range from 1028.5 to 1033 nm. By cooling the crystal under study to liquid nitrogen temperatures, the fraction of the absorbed output power η_g at 1030 nm decreased from 17 % at 293 K to $\eta_g < 2$ % at 80 K, which illustrates a decrease in the population of the lower working level according to the Boltzmann distribution.

When crystals were cooled, the curves $\sigma_{las}(\lambda)$ shifted and their shape, maximum values, and widths change. To calculate the stimulated emission cross section on the working transition at different temperatures, we measured the spontaneous emission spectrum of the 600-μm-thick crystal in the temperature region 80 K – 296 K. The obtained dependences of the stimulated emission cross section on the wavelength at different temperatures are presented in Fig. 7. The dependences are normalised so that the maximum cross section at 290 K be equal to $\sim 2 \times 10^{-20}$ cm^2 [9, 28]. The shift of the cross section maximum was ~ 0.3 nm (in [29] – 1 nm) and the cross section in the maximum increased not by eight times as in [29] but by four times, which agrees with the results of papers [7 – 9]. These data indicate the necessity of matching the wavelengths of the oscillator and amplifier even if they are made of identical crystals.

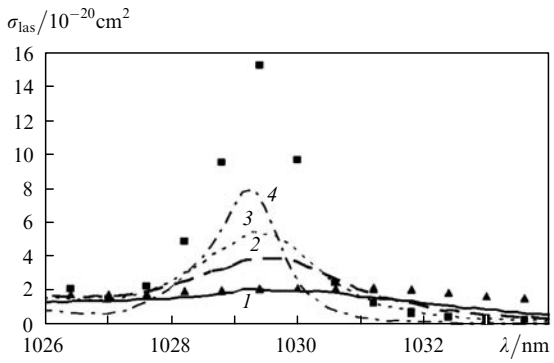

Figure 7. Wavelength dependences of the stimulated emission cross section at the working transition in the 10 % Yb-doped YAG crystal at 296 K (*1*), 210 K (*2*), 170 K (*3*) and 80 K (*4*). Dots are data from paper [29] obtained at 80 K (■) and 300 K (▲).

4.3 Gain as a function of the pump power

The experimentally measured dependences of the small-signal gain per two passes on the absorbed pump power in the 600-μm-thick crystal are presented in Fig. 8. The dependences were obtained for different wavelengths of the oscillator. Different positions of the maxima of these dependences indicate a decrease in the stimulated emission cross section and a shift in its maxima due to the crystal heating (section 3.1). The average crystal temperature was calculated in our experiments with the help of the methods from paper [30]. Using the data of Fig. 7, we calculated with the help of expressions from section 2 solid and dashed curves in Fig. 8. The dashed curve was plotted for the case, when, as in the experiment, a sapphire disk [(*3*) in Fig. 6] without a thermal contact with the copper heatsink [(*4*) in Fig. 6] and decreasing the average crystal temperature was fixed to the crystal face. In calculations the crystal temperature was assumed the same, over the entire volume, and the stimulated emission cross section at 290 K was $1.7\times\ 10^{-20}$ cm^2. The cross section was averaged with respect to the emission line of the oscillator. A small discrepancy of the theoretical results and the experiment is explained by the inaccuracy of data on the crystal temperature and the stimulated emission cross section as well as by the finite emission bandwidth of the oscillator.

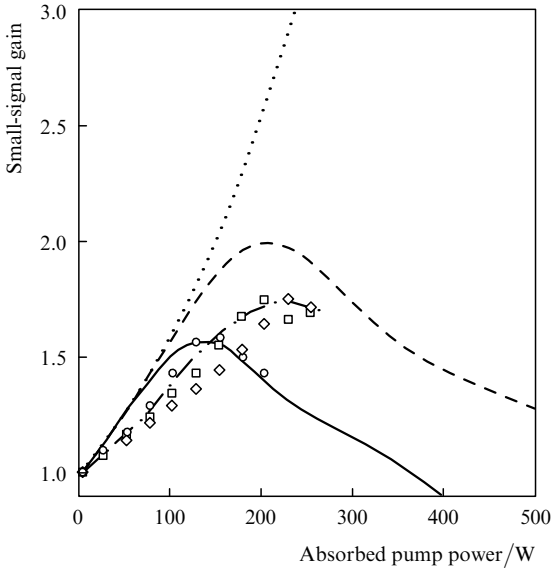

Figure 8. Small-signal gain per two passes in the 600-μm-thick Yb : YAG crystal as a function of the absorbed pump power at 80 K. Dots are the experimental results obtained at different oscillator wavelengths. The dash-and-dot curve is their envelope. The dashed and solid curves are the theoretical dependences in the presence of the sapphire disk (see the text) and in its absence, respectively. The dotted curve is the theoretical dependence neglecting the change in the crystal temperature in the case of the absorption of the pump power.

Taking into account these factors, the agreement of theoretical and experimental results can be treated as satisfactory.

5. Conclusions

We have studied theoretically and experimentally the main parameters of a double-pass disk diode-pumped Yb : YAG amplifier. A set of approximate solutions of the system of differential equations has been obtained for a four-level scheme of the amplifier with a monochromatic pump. The range of values of the parameters in which these or those solutions are valid, have been found. The most interesting is the solution with a partial account for the saturation effect, which well agrees with the exact numerical solution.

The derived expressions make it possible to estimate the optimal doping of the crystal by Yb ions, which is 10 % for a 600-μm-thick crystal.

In calculations we have taken into account the spectral characteristics of absorption in AEs and pump radiation (shape, width, central wavelength). The method of search for the optimal central pump radiation wavelength has been proposed. It has been shown that the account for the spectral characteristics is more important than saturation. The properties of the 600-μm-thick 10 % Yb-doped YAG crystal have been studied experimentally for the pump power up to 600 W both at room temperature and at 80 K. By cooling the crystal, we have observed the shift of the centre of the gain profile (~ 0.3 nm) and the increase in the stimulated emission cross section (by four times) as well as the depletion of the lower working level. The dependence of the small-signal gain (the maximum value is 1.7) on the absorbed pump power has been measured. The qualitative agreement of the experimental results with the theoretical calculations, taking into account the temperature dependences of spectral and thermal characteristics of Yb : YAG crystals, takes place.

On the whole the results of this paper show the possibility of manufacturing a cryogenic disk pulse periodic Yb : YAG laser with the pulse repetition rate 1 kHz, pulse energy 250 mJ and pulse duration 100 ps at the pump power 1 kW.

Acknowledgements. This work was supported by the program of the Presidium of the Russian Academy of Sciences 'Femtosecond Optics and New Optical Materials' and the Russian Foundation for Basic Research (Grant No. 08-02-99044-r_ofi).

References

1. Tavella F., Marcinkevicius A., Krausz F. *Opt. Express*, **14**, 12822 (2006).
2. Nakai S., Kanabe T., Kawashima T., Yamanaka M., Izawa Y., Nakatuka M., Kandasamy R., Kan H., Hiruma T., Niino M. *Proc. SPIE Int. Soc. Opt. Eng.*, **4065**, 29 (2000).
3. Kawashima T., Kanzaki T., Matsui H., Kanabe T., Yamanaka M., Izawa Y., Nakai S., Matsui K., Miyamoto M., Kan H., Hiruma T. *Proc. SPIE Int. Soc. Opt. Eng.*, **3889**, 596 (2000).
4. Bibeau C.M., Bayramian A.J., Beach R.J., Campbell R.W., DeWald A., Davis W.H., Dawson J.W., DiMercurio L.E., Ebbers C.A., Freitas B.L., Hill M.R., Hood K.M., Kanz K.V., Menapace J.A., Payne S.A., Randles M.H., Rankin J.E., Schaffers K.I., Stoltz C.J., Tassano J.B., Telford S.J., Utterback E.J. *Proc. SPIE Int. Soc. Opt. Eng.*, **5332**, 244 (2004).
5. Mezenov A.V., Soms L.N., Stepanov A.I. *Termooptika tverdotel'nykh lazerov* (Thermal Optics of Solid-State Lasers) (Leningrad: Mashinostroenie, 1986) p. 199.
6. Koechner W. *Solid-State Laser Engineering* (Berlin: Springer, 1999).
7. Bass M., Weichman L., Vigil S., Brickeen B.K. *IEEE J. Quantum Electron.*, **39**, 741 (2003).
8. Rapaport A., Zhao Z., Xiao G., Howard A., Bass M. *Appl. Opt.*, **41**, 7052 (2002).
9. Dong J., Bass M., Mao Y., Deng P., Gan F. *J. Opt. Soc. Am. B*, **20**, 1975 (2003).
10. Sennaroglu A. *Appl. Opt.*, **38**, 3253 (1999).
11. Krupke W. *IEEE J. Sel. Top. Quantum Electron.*, **6**, 1287 (2000).
12. Brown D.C. *IEEE J. Quantum Electron.*, **34**, 560 (1998).
13. Fan T.Y. *IEEE J. Quantum Electron.*, **29**, 1457 (1993).
14. Brown D.C., Bowman R., Kuper J., Lee K.K., Menders J. *Appl. Opt.*, **25**, 612 (1986).
15. Lee J.-C., Kelly J.H., Smith D.L., Jacobs S.D. *IEEE J. Quantum Electron.*, **24**, 2238 (1988).
16. Schulz P.A., Henion S.R. *IEEE J. Quantum Electron.*, **27**, 1039 (1991).
17. Ripin D.J., Ochoa J.R., Aggarwal R.L., Fan T.Y. *Opt. Lett.*, **29**, 2154 (2004).
18. Backus S., Bartels R., Thompson S., Dollinger R., Kapteyn H.C., Murnane M.M. *Opt. Lett.*, **26**, 465 (2001).
19. Tokita S., Kawanaka J., Fujita M., Kawashima T., Izawa Y. *Appl. Phys. B*, **80**, 635 (2005).
20. Brown D.C. *IEEE J. Sel. Top. Quantum Electron.*, **11**, 587 (2005).
21. Tokita S., Kawanaka J., Izawa Y., Fujita M., Kawashima T. *Opt. Express*, **15**, 3955 (2007).
22. Cai H., Zhou J., Zhao H., Qi Y., Lou Q., Dong J., Wei Y. *Chin. Opt. Lett.*, **6**, 852 (2008).
23. Bahbah S., Albach D., Assemat F., Bourdet G., Chanteloup J.-C., Piatti P., Pluvinage M., Vincent B., Touzé G.L. *J. Phys. Conf. Ser.*, **112**, 032053 (2008).
24. Brasseur J.K., Abeeluck A.K., Awtry A.R., Meng L.S., Shortoff K.E., Miller N.J., Hampton R.K., Cuchiara M.H., Neumann D.K. *Proc. SPIE Int. Soc. Opt. Eng.*, **6952**, 69520L (2008).
25. Frantz L.M., Nodvik J.S. *J. Appl. Phys.*, **34**, 2346 (1963).
26. Brown D.C., Cone R.L., Sun Y., Equall R.W. *IEEE J. Sel. Top. Quantum Electron.*, **11**, 604 (2005).
27. Baum A., Grebner D., Paa W., Triebel W., Larionov M., Giesen A. *Appl. Phys. B*, **81**, 1091 (2005).
28. Giesen A., Hugel H., Voss A., Witting K., Brauch U., Opower H. *Appl. Phys. B*, **58**, 365 (1994).
29. Tokita S., Kawanaka J., Fujita M., Kawashima T., Izawa Y. *Techn. Dig. CLEO/QELS'2006* (Long Beach, Cal., USA, 2006); http://lasers.llnl.gov/programs/psa/pdfs/hec-dpssl06/05picose-cond.pdf.
30. Vyatkin A.G., Khazanov E.A. *Kvantovaya Elektron.*, **39**, 814 (2009) [*Quantum Electron.*, **39**, 814 (2009)].